Chapter 4
$A + B \rightarrow C$ Reaction Fronts in Hele-Shaw Cells Under Modulated Gravitational Acceleration

Laurence Rongy, Kerstin Eckert, and Anne De Wit

Abstract We study the dynamics of $A + B \rightarrow C$ reaction fronts propagating under modulated gravitational acceleration by means of parabolic flight experiments and numerical simulations. We observe an accelerated front propagation under hypergravity along with a slowing down of the front under low gravity. By reaction-diffusion-convection simulations of an $A + B \rightarrow C$ front propagating in a thin layer, we can relate this periodic modulation of the front position to the amplification and decay, respectively, of the buoyancy-driven double vortex associated with the front propagation. A correlation between grey-value changes in the experimental shadowgraph images and characteristic changes in the concentration profiles are obtained by a numerical simulation of the imaging process (Eckert et al., Phys. Chem. Chem. Phys., 14:7337–7345, 2012).

4.1 Background

In a variety of chemical systems, buoyancy-driven convection has been shown to remarkably influence the propagation of reaction fronts. For example, the propagation speed of autocatalytic fronts in capillary tubes depends on the angle of inclination of the tube with regard to the vertical [2]. Simpler and more common chemical reaction types than autocatalysis are second-order irreversible reactions of the form $A + B \rightarrow C$. Provided that the two reactants A and B are initially separated in space, a reaction front can also propagate in these chemical systems. It has recently been shown that the reaction-diffusion properties of such fronts [3, 4] are not recovered if they develop in thin horizontal liquid layers where gravity points across the thin layer [5]. This suggests that the dynamics of these fronts can be influenced by chemically-driven buoyancy convection if A, B, and C have different densities. Rongy et al. [6, 7] have shown numerically that the nonlinear dynamics is characterized by one or two flow vortices developing around the front in covered horizontal

L. Rongy (✉) · A. De Wit
Nonlinear Physical Chemistry Unit, Service de Chimie Physique et Biologie Théorique, Faculté des Sciences, Université Libre de Bruxelles (ULB), CP 231, 1050 Brussels, Belgium

K. Eckert
Institute of Fluid Mechanics, Technische Universität Dresden, 01062 Dresden, Germany

Fig. 4.1 *Top*: Sketch of the reaction-diffusion profiles in the reactive liquid-liquid system. *Bottom*: Velocity field superimposed on salt concentration field ranging from $s = s_{\max}$ in *the middle* (*red*) to $s = 0$ on the sides (*blue*) in the hyper-gravity phase. The maximum intensity of the velocity vectors is 1.1 in dimensionless units
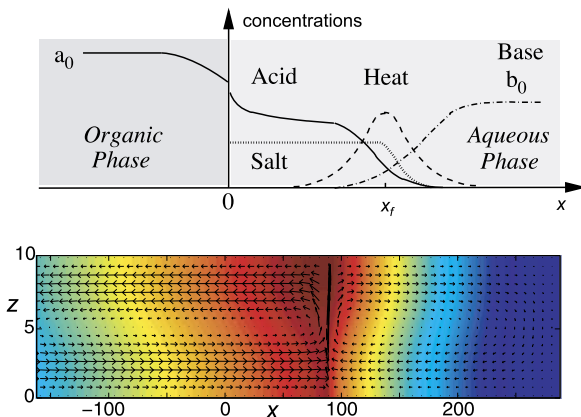
layers. They have furthermore classified the various possible density profiles and related flow properties in a parameter space spanned by the three Rayleigh numbers of the problem. We provide here a direct comparison between experiments and these theoretical predictions. We show moreover that they can be used to understand situations on earth but also more complicated scenarios with modulated gravity, such as the ones observed in parabolic flights.

4.2 Chemical System and Model

The experimental container is a Hele-Shaw (HS) cell where propionic acid (A) undergoes a mass transfer from an organic phase (cyclohexane) into the aqueous layer and is subsequently neutralised by the base TMAH (B), producing a salt, tetramethylammonium propionate (C), according to $A + B \rightarrow C$ (see Fig. 4.1). The reaction front in the HS cell is followed by means of the shadowgraph technique [9]. This technique is sensitive with respect to the Laplacian of the refractive index n and the shadowgraph produces a relative change in the light intensity, from which the reaction front position X_f can be extracted. In ground experiments the resulting hydrodynamic instabilities have been well characterized [5, 8] and we focus here on microgravity situations.

To reduce complexity, the simulations focus entirely on the aqueous phase, instead of treating the complete liquid-liquid system with the mass transfer through the interface. This is justified because, after some minutes only, the reaction front is already sufficiently far from the interface. Thus we consider a two-dimensional (2D) thin aqueous solution layer placed horizontally in the gravity field in which an acid-base reaction, $A + B \rightarrow C$, takes place. The governing equations for the acid, base, and salt concentrations are isothermal reaction-diffusion-convection equations. The evolution of the 2D velocity field, $\vec{v}$, is described by the incompressible Stokes equations and is coupled to the evolution of the concentrations through an equation of state. In the latter we assume a linear dependence between the solution density, ρ,

Fig. 4.2 Flight protocol of the normalized magnitude of the gravitational acceleration, g/g_0 with $g_0 = 9.81$ m/s^2, versus time, as used in the simulations
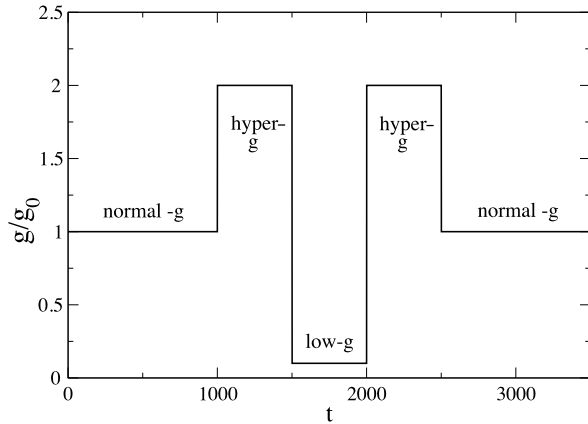
and the concentrations, introducing Rayleigh numbers directly proportional to the experimental contribution of each species to the changes in density. To simulate the gravity modulations of the parabolic flight we let the normalized magnitude of the gravitational acceleration, g/g_0 , with $g_0 = 9.81$ m/s^2, vary with time following the flight protocol (see Fig. 4.2).

4.3 Experimental and Numerical Results

When two miscible solutions containing A and B, respectively, are brought into contact, the dynamics of the $A + B \rightarrow C$ fronts developing in the liquid layer measured experimentally during parabolic flights differ from those obtained on earth [5]. This confirms that, even in thin liquid layers, convective motions can influence the properties of such fronts drastically. When gravitational acceleration varies periodically, we observe an associated periodic change between an accelerated front propagation under hyper-gravity and a slowed down propagation under low gravity. These results are explained by the numerical integration of our reaction-diffusion-convection model. The simulations reproduce the experimental behavior and allow to relate the modulation of the front position to the changes in the buoyancy-driven flow field consisting of a double vortex (see Fig. 4.1). This vortex consists of a rising flow at the reaction front, advecting fresh reactants towards it. The amplification or decay of such a double vortex when increasing or decreasing the g-level, respectively, explains the periodic behavior of the front position.

Figure 4.3 indicates a representation of the reaction front under parabolic flight conditions by two characteristic lines, the leading edge (LE) and the trailing edge (TE) (see caption of Fig. 4.3). The width of the front, defined as the distance between these two lines, is maximum in the low-gravity phase and minimum in the hyper-gravity phase. Thanks to the numerical simulations of the experimental shadowgraph visualization, we are able to interpret the meaning of LE and TE and to establish a correlation between the changes of the grey values in the experimental

Fig. 4.3 Shadowgraph images of the system during the three characteristic stages of the parabolic flight: normal-gravity, hyper-gravity, and low-gravity phases. The position of the front is followed to two characteristic lines, TE and LE. TE corresponds to the trailing edge, which is the brightest contour of the shadowgraph, and LE is the leading edge, which is the darkest contour and is directed towards the fresh aqueous phase
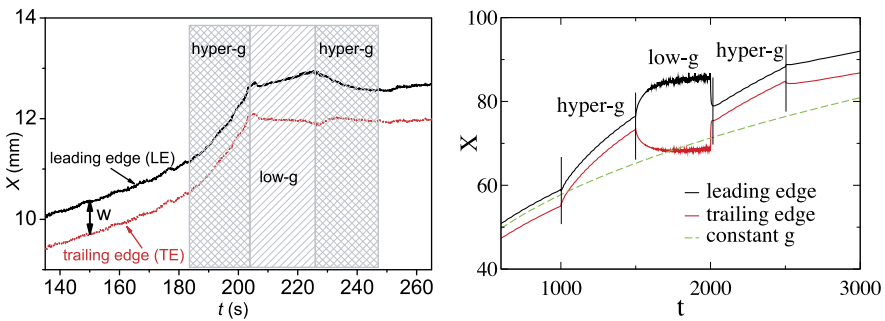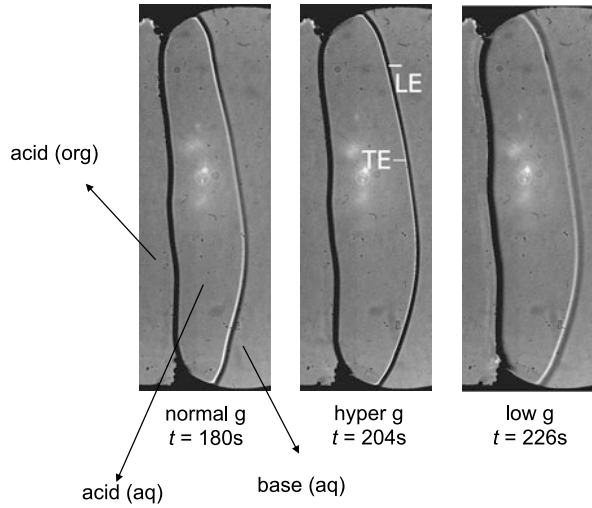

Fig. 4.4 Experimental (*left*) and numerical (*right*) behavior of the positions X_f^{LE} and X_f^{TE} of leading and trailing edges versus time during different stages of one parabola

images with those of the concentration fields. In particular, the observation of an increasing front width at decreased contrast during the low-gravity phase can be related to a change in the curvature of the concentration profiles. Indeed, the positions of the leading and trailing edges are deduced from the positions of minimum and maximum $d^2\langle n \rangle / dx^2$ during one period of g-modulation, where n, the refractive index, is reconstructed from the numerical concentration profiles as a linear combination of the concentration fields of each species.

Figure 4.4 illustrates the behavior of the two characteristic lines, LE and TE, during the different stages of the parabolic flight. There is an excellent qualitative agreement between the experimental and numerical results. In the numerical part of Fig. 4.4 we also evidence the acceleration of the reaction front in the parabolic flight conditions compared to the situation under constant normal gravity $g = 1g_0$.

References

1. Eckert K, Rongy L, De Wit A (2012) $A + B \rightarrow C$ reaction fronts in Hele-Shaw cells under modulated gravitational acceleration. Phys Chem Chem Phys 14:7337–7345
2. Nagypal I, Bazsa G, Epstein IR (1986) Gravity-induced anisotropies in chemical waves. J Am Chem Soc 108:3635–3640
3. Gálfi L, Rácz Z (1988) Properties of the reaction front in an $A + B \rightarrow C$ type reaction-diffusion process. Phys Rev A 38:3151–3154
4. Jiang Z, Ebner C (1990) Simulation study of reaction fronts. Phys Rev A 42:7483–7486
5. Shi Y, Eckert K (2006) Acceleration of reaction fronts by hydrodynamic instabilities in immiscible systems. Chem Eng Sci 61:5523–5533
6. Rongy L, Trevelyan PMJ, De Wit A (2008) Dynamics of $A + B \rightarrow C$ reaction fronts in the presence of buoyancy-driven convection. Phys Rev Lett 101:084503
7. Rongy L, Trevelyan PMJ, De Wit A (2010) Influence of buoyancy-driven convection on the dynamics of $A + B \rightarrow C$ reaction fronts in horizontal solution layers. Chem Eng Sci 65:2382–2391
8. Eckert K, Acker M, Shi Y (2004) Chemical pattern formation driven by a neutralization reaction. I: Mechanism and basic features. Phys Fluids 16:385–399
9. Merzkirch W (1987) Flow visualization. Academic Press, New York